The moments of the PDF of concentration for gas clouds in the presence of fences (*)

P. C. CHATWIN and C. ROBINSON
School of Mathematics and Statistics, University of Sheffield
P.O. Box 597, Sheffield S10 2UN, UK

(ricevuto il 10 Gennaio 1996; revisionato il 17 Marzo 1997; approvato il 10 Aprile 1997)

Summary. — A team led by D. J. Hall has conducted many trials, each involving the instantaneous release of a heavy or neutrally buoyant gas in the presence of a fence aligned transverse to the mean flow, thus complementing earlier trials without fences. For each fence and for each Richardson Number Ri, at least 50 repetitions of each release were performed. This allowed estimates to be made of some statistical properties (mean concentration μ, standard deviation σ, skewness S, kurtosis K), and their variation with time. Typical results are presented and discussed. The strongest influence of the fences on the evolution of μ and σ with time is vertical mixing, but there are also interesting changes with fence height and type, and with Ri. The possibility of a relationship between μ and σ is discussed. However, the most remarkable result is, perhaps, that the estimates of S and K are such that, in all cases, the (K, S) plot collapses onto a quadratic curve; this extends the same finding earlier by Mole and Clarke for steady releases and, in particular, suggests strongly that the PDF of concentration is, in practice, determined by only three properties, *e.g.* (μ, σ, S).

PACS 96.60.Ek – Convection, turbulence, and diffusion.
PACS 12.60.Sz – Air qulity and air pollution.
PACS 01.30.Cc – Conference proceedings.

1. – Introduction

When a scalar contaminant is released into, and dispersed by, a turbulent flow, its concentration $\Gamma(\mathbf{x}, t)$ is a random function of position $\mathbf{x}$ and time t. In most cases,

(*) Paper presented at EUROMECH Colloquium 338 “Atmospheric Turbulence and Dispersion in Complex Terrain” and ERCOFTAC Workshop “Data on Turbulence and Dispersion in Complex Atmospheric Flows”, Bologna, 4-7 September 1995.

including those examined in this paper, Γ satisfies the equation

$$\frac{\partial \Gamma}{\partial t} + \mathbf{Y}\cdot\nabla\Gamma = \kappa\nabla^2\Gamma\,, \tag{1}$$

where the constant κ is molecular diffusivity and $\mathbf{Y} = \mathbf{Y}(\mathbf{x}, t)$ is the random (turbulent) velocity which (in turn) satisfies the Navier-Stokes, and mass conservation, equations. The quantitative features of the statistical properties of the randomness, or natural variability, of Γ are therefore controlled by the physics described by these equations, and these properties are of considerable practical and theoretical interest.

Many experimental investigations of these properties have been undertaken. In most of these, the contaminant was released at a constant rate into the flow. In such circumstances, the statistical properties of Γ, such as the mean μ and variance σ^2 of Γ and its PDF (probability density function) p, are independent of t if those of the turbulent flow field are. But in most cases of practical interest, such releases are unrealistic since the contaminant enters the flow at a time-varying rate as, for example, in accidents.

To some extent, this fault was rectified recently in Project BA, supported by the EU (European Union) as part of its MTH (Major Technological Hazards) programme. A team led by Dr David Hall ([1]) undertook two extensive wind-tunnel investigations with instantaneous releases. The first series of experiments [1] was over unobstructed terrain; they have been analysed in many papers, including Davies [2], Zimmerman and Chatwin [3] and Sweatman and Chatwin [4]. The present paper deals with the second series of experiments [5] in which fences of different types were placed across the flow downwind of the source.

2. – Experimental details

The wind tunnel has a working section of length 22.0 m, width 4.3 m and height 1.5 m. In all cases, the contaminant was a gas which, before release, was confined to a source in the form of a cylindrical tent of diameter 0.14 m and height 0.13 m, the centre of whose base was located on the centre-line of the floor of the working section. Essentially instantaneous release was effected at time $t = 0$ by very rapidly collapsing the tent wall (in about 0.2 s) into the floor, leaving the roof behind supported by three thin vertical rods; the gas was then free to disperse. As explained in [1] and [5], this size and shape were chosen so that the source was an exact 1:100 scale model of that used in the Thorney Island trials [6]. The arrangement is shown in fig. 1, adapted from [5].

Measurements of Γ as a function of time t were made at 4 stations downwind of the source. With (x, y, z) denoting downwind distance, crosswind distance and height above the floor respectively, these were located at (70, 0, 0.4) cm, (70, 0, 2.4) cm, (200, 0, 0.4) cm and (200, 0, 2.4) cm. Two types of fence, solid and crenellated, were used, but the fence was always 100 cm downwind of the source and always of length 4.3 m (so that it spanned the whole working section). Figure 1 shows also the

([1]) The experiments were conducted at Warren Spring Laboratory which the UK Government has since closed. Enquiries about the "reasons" for the closure of Warren Spring Laboratory should be directed to the UK Government and not to Dr Hall.

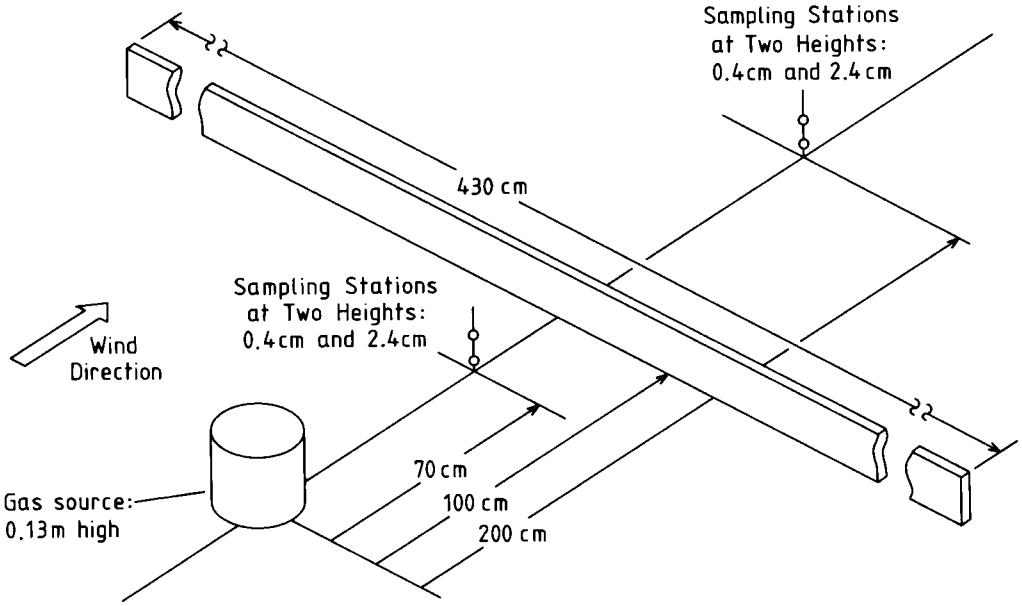

Fig. 1. – The experimental configuration showing a solid fence in position. Adapted from [5].

measuring stations, and a solid fence in position. Figure 2 indicates the geometry of the crenellated fences which were made of square segments separated by a distance equal to the height of each segment (so that the fence solidity was 50%). In all experiments using a crenellated fence, it was located spanwise so that a gap was directly downwind of the source, tests having suggested that results would not be significantly different if, instead, a solid element was directly downwind. The fence height H was varied, with 6 values ($H = 1.6$, 3.8, 5.1, 7.6, 10.2, 15.3 cm) for solid fences and 3 values ($H = 3.8$, 7.6, 15.3 cm) for crenellated fences.

Also varied systematically was the density of the source gas, although it was never less than that of the ambient air. This is in recognition of the fact that many potential accidents involve the release of heavy gases. If the density of the gas at release is $\varrho + \Delta\varrho$, where ϱ is the density of the ambient air, the non-dimensional Richardson number Ri is defined by

$$\mathrm{Ri} = \frac{g \cdot \Delta\varrho \cdot L}{\varrho U^2} \,, \tag{2}$$

where g is the acceleration due to gravity, $L = 0.13$ m is the height of the cylindrical source, and U is the mean wind speed at height L. Measurements in the presence of fences were made for $\mathrm{Ri} = 0$ (neutrally buoyant, or passive, release), 1, 2, 5, 10. When $\mathrm{Ri} > 0$, there are negative buoyancy force terms in the Navier-Stokes equations and $\mathbf{Y}(\mathbf{x}, t)$ is changed from its value when $\mathrm{Ri} = 0$; the structure of eq. (1) is, however, not changed. The Thorney Island trial results and those in the wind tunnel reported in [1] showed that when $\mathrm{Ri} > 0$ the gas cylinder initially collapsed under gravity and (with this release mechanism at least) tended to form a “doughnut” before being advected

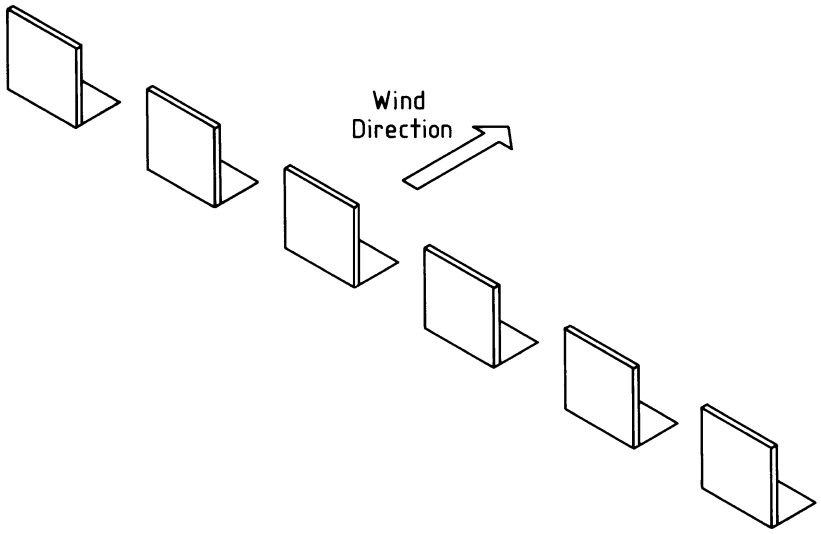

Fig. 2. – The geometry of the crenellated fences. Adapted from [5].

downwind and dispersed by the ambient flow. This doughnut leads, in effect, to some upwind dispersion and this is apparent in fig. 3.

Table I shows all 33 experimental configurations that were used, where those for $H/L = 0$ (*i.e.* no fence) occurred in the first series [1]. Those in this first series with $\mathrm{Ri} = 0.5$ are not considered here since this value was not used in the second series with fences. In order to allow reasonable estimates of statistical properties to be made, each of the 28 releases with fences was repeated 50 times as were those with no fence for

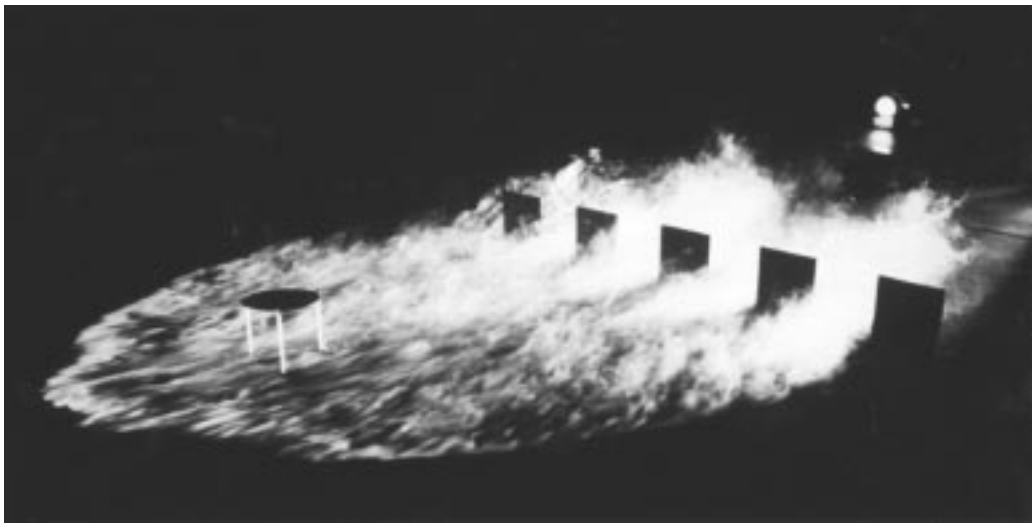

Fig. 3. – A typical view of dispersion soon after release in the presence of a crenellated fence ($\mathrm{Ri} = 10$, $H = 15.3$ cm). See text for further details.

TABLE I. – *The experimental configurations used are indicated by* √, *where* S, C *denote solid fence and crenellated fence respectively.* $L = 0.13$ m *is the height of the cylindrical source and* H *is the height of the fence* (*see text for values*).

Ri	H/L												
	0	0.12		0.3		0.4		0.6		0.8		1.2	
	No fence	S	C	S	C	S	C	S	C	S	C	S	C
0	√	×	×	×	√	√	×	√	√	√	×	√	√
1	√	×	×	√	×	×	×	√	×	×	×	√	×
2	√	×	×	√	√	×	×	√	√	×	×	√	√
5	√	×	×	√	×	×	×	√	×	×	×	√	×
10	√	√	×	√	√	√	×	√	√	√	×	√	√

Ri = 5, 10. Those with no fence for Ri = 0, 1, 2 were repeated 100 times. In addition, some flow visualisation studies were performed and summaries of the results are discussed in [5].

3. – Purpose of data analysis

For each experimental configuration in table I, and for each of the four stations, Γ is a random variable and, moreover, its statistical properties evolve systematically with time t. This is clear from fig. 4, which is entirely typical in these respects. There is a period after release before the gas cloud reaches the sensor, and the duration of this period is a principal random feature of the process [3]. The value of Γ rises very rapidly to a local maximum as the cloud reaches the sensor and then evolves with time, eventually reaching zero once all the gas has been advected downwind of the sensor. But, as the marked differences between the 25 replications in fig. 4 show, this overall behaviour is accompanied by large random fluctuations.

Therefore, since $\Gamma(\mathbf{x}, t)$ is a random variable, it has a PDF $p = p(\theta; \mathbf{x}, t)$ satisfying

$$p(\theta; \mathbf{x}, t) = \frac{\mathrm{d}}{\mathrm{d}\theta} \operatorname{prob}[\Gamma(\mathbf{x}, t) \leqslant \theta], \tag{3}$$

or, equivalently (for $\delta\theta$ small and positive),

$$p(\theta; \mathbf{x}, t)\, \delta\theta \approx \operatorname{prob}[\theta \leqslant \Gamma(\mathbf{x}, t) \leqslant \theta + \delta\theta]. \tag{4}$$

In eqs. (3) and (4), θ is non-negative and denotes the range of values that $\Gamma(\mathbf{x}, t)$ can take. For these experimental configurations, p depends explicitly on t as fig. 4 clearly shows. Moreover, it is precisely determined by the physics, including eq. (1), but it is not known how to carry out this determination [14]. From the experimental viewpoint, the data available for each of the 4 values of $\mathbf{x}$ at which measurements were taken is 50 (or, in three cases, 100) values of Γ for each time t. As the analysis in [3]

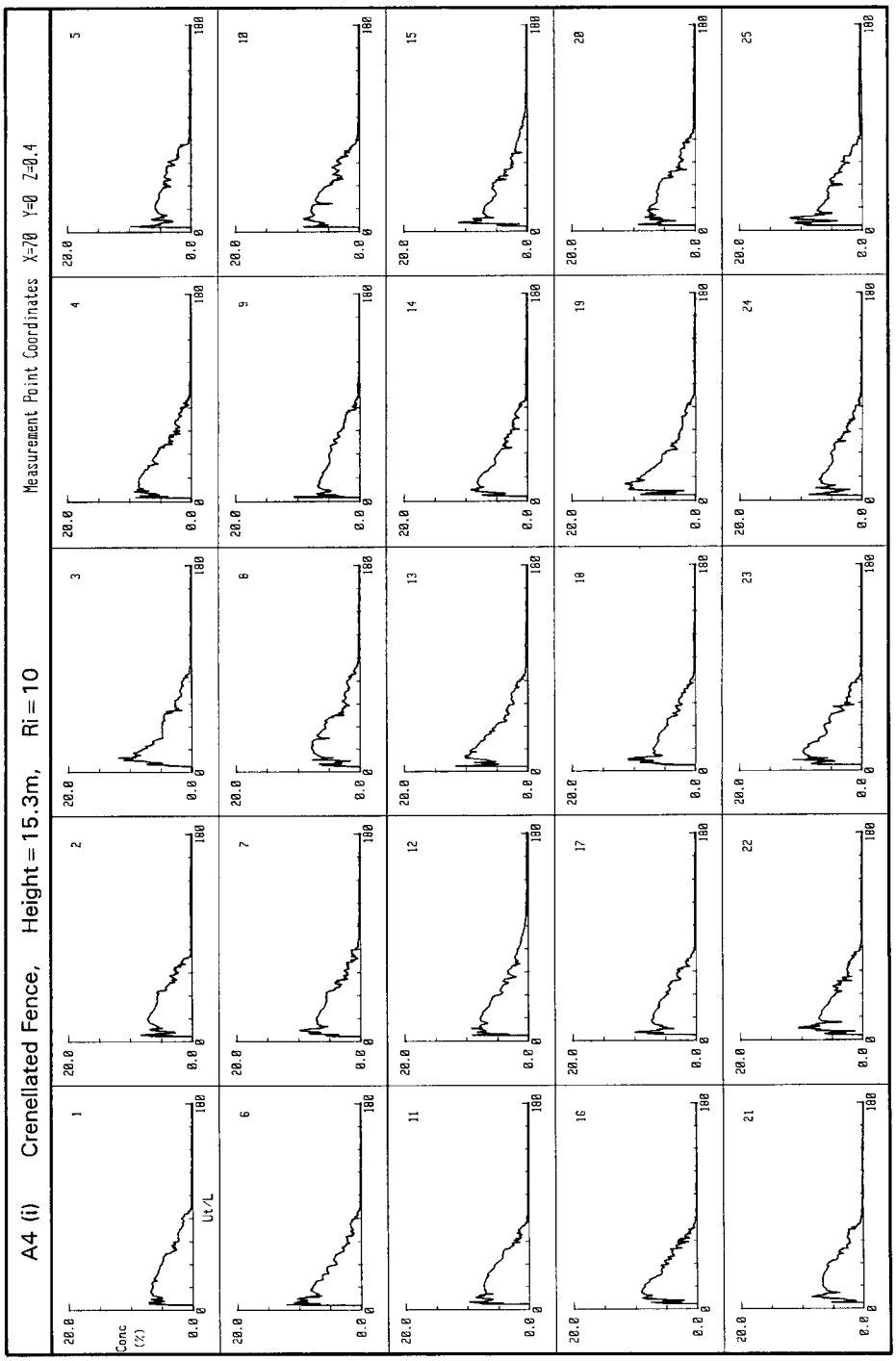

Fig. 4. – The time series of Γ for the first 25 (out of 50) replications at the lower upwind station in the presence of a crenellated fence when Ri = 10 and H = 15.3 cm—the case illustrated in fig. 3. (This is fig. A4(i) of [5].)

shows, neither number of replications is sufficient to estimate $p(\theta; \mathbf{x}, t)$ reliably or satisfactorily because any estimate is swamped by statistical noise.

Fortunately, there are simpler, but important, statistical properties of $\Gamma(\mathbf{x}, t)$ that can be estimated much more reliably than $p(\theta; \mathbf{x}, t)$ and these will be the concern of the remainder of this paper. Foremost, perhaps, amongst these properties is the mean concentration $\mu(\mathbf{x}, t)$ related to $p(\theta; \mathbf{x}, t)$ by

$$\mu(\mathbf{x}, t) = \int_0^\infty \theta p(\theta; \mathbf{x}, t)\, \mathrm{d}\theta \,. \tag{5}$$

The value of $\mu(\mathbf{x}, t)$ is also known as the expected value of $\Gamma(\mathbf{x}, t)$ and this term clearly denotes its practical significance. The other properties that will be considered are some of the central moments $\mu_n(\mathbf{x}, t)$ where $n > 1$ and

$$\mu_n(\mathbf{x}, t) = \int_0^\infty [\theta - \mu(\mathbf{x}, t)]^n p(\theta; \mathbf{x}, t)\, \mathrm{d}\theta \,. \tag{6}$$

In particular, the variance σ^2, skewness S and kurtosis K satisfy

$$\sigma^2 = \mu_2, \qquad S = \frac{\mu_3}{\sigma^3}, \qquad K = \frac{\mu_4}{\sigma^4} \,. \tag{7}$$

The value of $\sigma = \sigma(\mathbf{x}, t)$ is the standard deviation (or rms fluctuation value) of $\Gamma(\mathbf{x}, t)$ and is a measure of the spread about $\mu(\mathbf{x}, t)$ that measured values of $\Gamma(\mathbf{x}, t)$ will take. Derksen and Sullivan [7] have shown that, in certain circumstances, good estimates of $p(\theta; \mathbf{x}, t)$ can be obtained from knowledge of μ, σ^2, S and K but, as explained above, the present data do not allow direct and reliable estimation of $p(\theta; \mathbf{x}, t)$ so this important possibility cannot be explored further.

Suppose that $\Gamma^{(r)}(\mathbf{x}, t)$ is the measured value of Γ at time t after instantaneous release at the station at $\mathbf{x}$ in the r-th replication ($r = 1, 2, \ldots, N$, where $N = 50$ or 100). Then, as is well-known, $\mu(\mathbf{x}, t)$ in eq. (5) can be estimated by

$$N^{-1} \sum_{r=1}^{N} \Gamma^{(r)}(\mathbf{x}, t) \,,$$

and there are corresponding expressions for estimating μ_n in eq. (6). But note that, unlike μ and μ_n, such expressions are themselves random variables containing statistical noise which is likely to decrease as N increases, and is likely to be greater for estimates of μ_n than of μ_m, where $n > m$. The presence of statistical noise will be evident in the graphs that are discussed later.

The aim of this work is to try to understand how the evolution with t of μ and the central moments is affected by fence height and type, by Ri, and by position. Therefore, for each of the 33 experimental configurations (see table I) and for each of the 4 sensor stations, estimates of μ, σ, S (obtained as indicated above) against t were plotted. Additionally, for reasons to be indicated later, graphs of σ *vs.* μ, and K *vs.* S, were plotted. There is obviously neither time nor space here for a full analysis of all 792 graphs; therefore this paper focuses only on certain points of interest. Further details, and all plots, are given in [8]. It should also be noted that the present analysis differs from, but complements, that in [5].

4. – Results and discussion

4·1. *Basic features.* – The flow visualisation studies in [5] show several important effects of the fences. These include:

i) All fences cause additional vertical mixing but no additional lateral spreading.

ii) The lateral spread for heavy clouds is much greater than that for neutrally buoyant clouds and is dominated by the effects of the initial gravitational collapse [1].

iii) For solid fences, neutrally buoyant clouds are advected over the fence without delay whereas heavy clouds tend to halt at the base and are subject to vertical mixing as they are carried over the fence relatively slowly.

iv) Having passed over a solid fence, gas clouds (both heavy and neutrally buoyant) are not entrained immediately into the separation region; there is some limited entrainment from the downwind end of this region.

v) For crenellated fences most of the gas passes through the gaps and is immediately diffused over the whole depth of the fence.

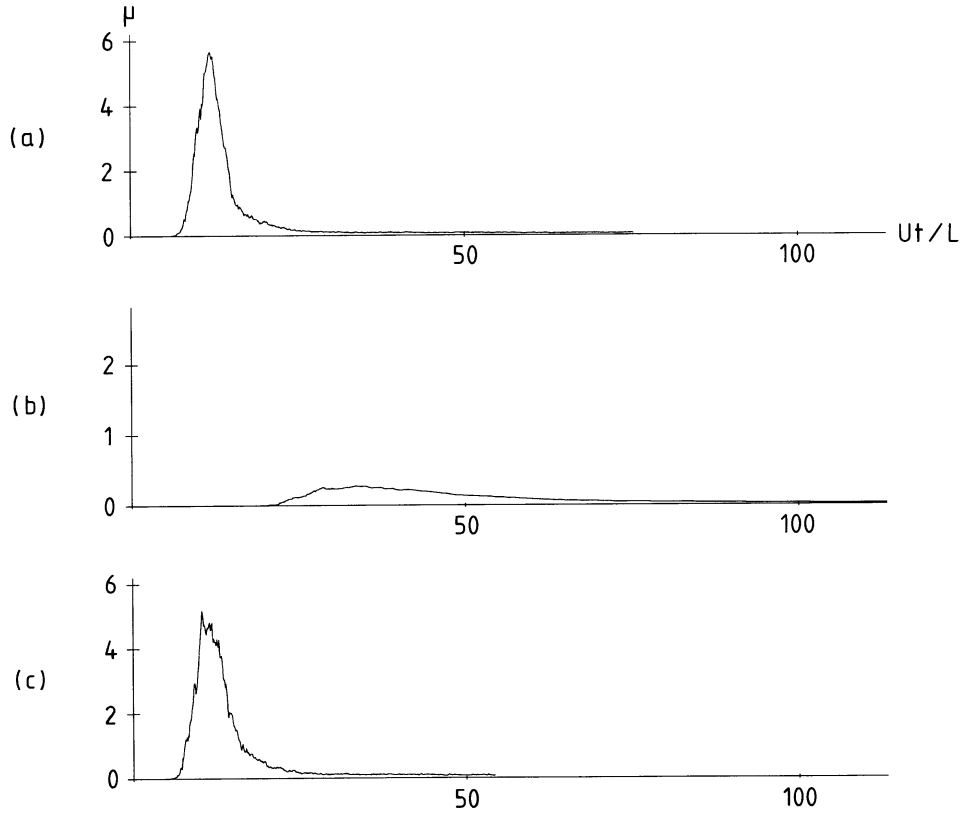

Fig. 5. – Three typical plots of μ (%) against Ut/L for neutrally buoyant ($\mathrm{Ri} = 0$) clouds. (a) No fence. (70, 0, 2.4) cm. (b) Solid fence, $H = 15.3$ cm. (200, 0, 0.4) cm. (c) Crenellated fence, $H = 7.6$ cm. (70, 0, 2.4) cm.

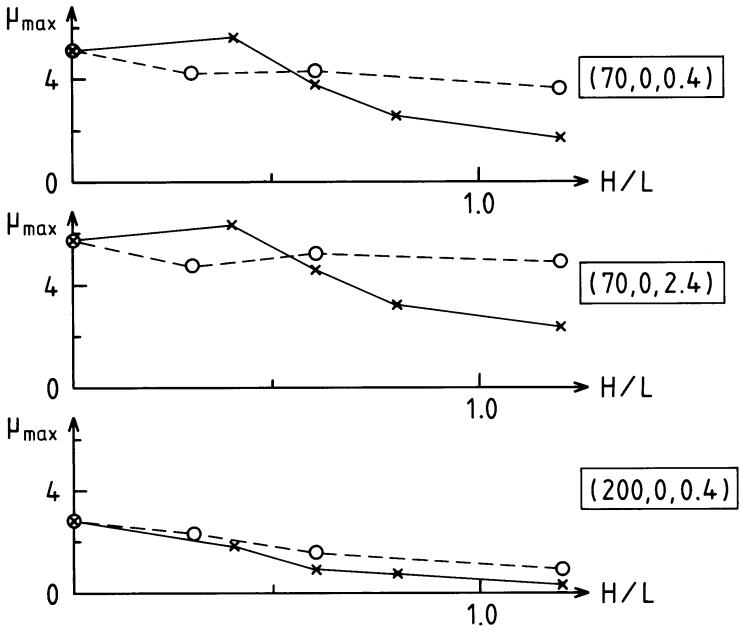

Fig. 6. – The variation of μ_{max}, the maximum mean concentration, with fence height H and type when Ri = 0 at three stations whose positions are indicated at the right-hand side of each plot. (As noted in the text following eq. (2), $L = 0.13$ m is the height of the source.) The variation at (200, 0, 2.4) cm is not shown, since it is very like that at (200, 0, 0.4) cm. The crosses (solid line) and circles (dashed line) denote solid and crenellated fences respectively.

4·2. *The effects of fences on the mean concentration.* – For neutrally buoyant clouds the graph of μ against t at each sensor is always unimodal (ignoring here, and later, small blips that are almost certainly due to statistical noise). This is true irrespective of fence presence or type as is illustrated by the three typical plots in fig. 5. The vertical mixing due to the fences increases in intensity with fence height H, and this causes the size μ_{max} of the maximum of μ at both downwind stations to decrease as H increases. For the upwind stations, the tendency for μ_{max} to be reduced by increased mixing immediately upwind of the fence is opposed to some extent by the upwind displacement of the gas as it is carried over the fence ([5]; figs. 7 and 11). The first two plots in fig. 6 show that the first of these effects is the stronger except for the lowest solid fence ($H/L = 0.4$). It is interesting that the reduction in μ_{max} at both upwind stations appears to be independent of H for crenellated fences, whereas μ_{max} steadily decreases with H for solid fences from its value for $H/L = 0.12$.

The behaviour of μ against t for the lightest of the dense gas clouds (Ri = 1) is not markedly different from that for Ri = 0. Here it suffices to note the profile in fig. 7, which is the only one to show the bimodal structure that is much more prominent at higher Ri (see below). Zimmerman and Chatwin [3] argued that the first maximum arises from the leading edge of the doughnut breaking away through entrainment by the ambient flow, and the second corresponds to the arrival of the bulk of the doughnut.

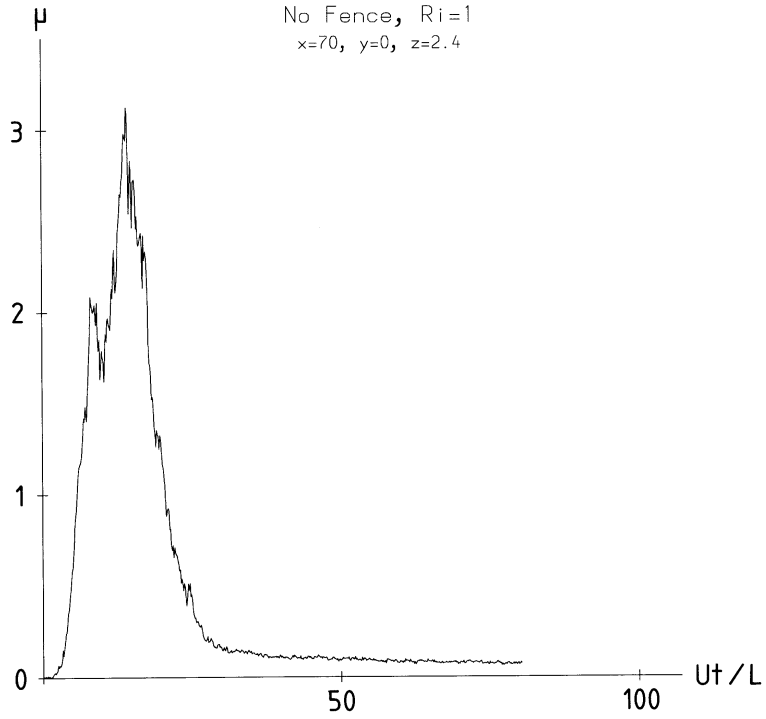

Fig. 7. – Ri = 1, (70, 0, 2.4) cm. No fence. The evolution of μ (%) with Ut/L.

Consistent with other findings reported by Hall *et al.* ([1], [5]), dense gas effects on μ become clearly noticeable for $\mathrm{Ri} \geqslant 2$. At both upwind stations the profile of μ against t at both $\mathrm{Ri} = 2$ and $\mathrm{Ri} = 5$ is nearly always bimodal as the eight typical plots in fig. 8 indicate (which are all for $\mathrm{Ri} = 2$, but $\mathrm{Ri} = 5$ plots are very similar). Occasionally one of the maxima is hardly discernible, or even absent; this may be genuine or could be due to statistical noise arising particularly from the large variability in arrival times (noted above). Stratification within the cloud (which is in the doughnut form immediately after release) causes the values of μ at the lower upwind sensor to be substantially greater than that at the upper upwind sensor, unlike the case when $\mathrm{Ri} = 0$ (see fig. 6). There is a clear tendency, illustrated in the relevant plots in fig. 8, for the second maximum at both upwind stations to become broader and higher as fence height increases. The most likely cause is the increased mixing due to the fence, which will not only reduce variations within the bulk of the cloud in each realisation but is also likely to weaken the leading edge. For solid fences, in addition, there is also the effect of the increased lift required to surmount the fence as H increases, thereby displacing the cloud position relative to the sensors. At both downwind stations, the graph of μ against t is always unimodal; the shape is always very similar to that in fig. 5(b) (although $\mu_{\max}$ values are lower than for $\mathrm{Ri} = 0$, presumably as a legacy of the extra mixing that heavy gas clouds undergo immediately after release). Figure 9 is interesting because it shows that $\mu_{\max}$ decreases significantly in the presence of a fence, but that, at all stations, the magnitude of the decrease is independent (to a first approximation at least) of both fence height and type. Although the mechanics of passing a fence is very different for

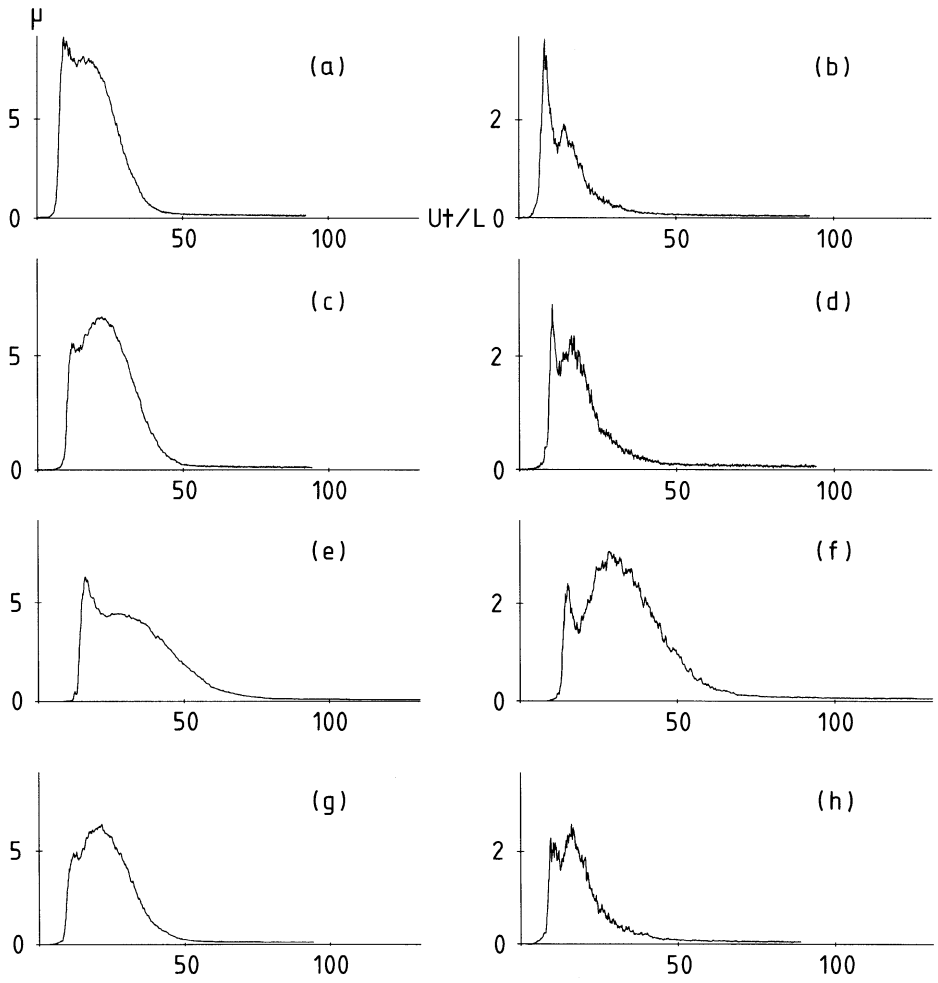

Fig. 8. – Ri = 2. Eight typical plots of μ (%) against Ut/L at the two upwind stations. The plots on the left ((a), (c), (e) and (g)) are from (70, 0, 0.4) cm, and those on the right ((b), (d), (f) and (h)) are from (70, 0, 2.4) cm. (a) and (b) no fence. (c) and (d) solid fence, $H = 3.8$ cm. (e) and (f) solid fence, $H = 15.3$ cm. (g) and (h) crenellated fence, $H = 7.6$ cm.

solid fences than for crenellated fences, this difference has little effect on $\mu_{\max}$, whose value is controlled by the additional mixing, however this is caused and whatever its precise features.

Several of the features just discussed are, not surprisingly, even more marked for Ri = 10. Figure 10 contrasts, for Ri = 10 and the highest solid fence ($H/L = 1.2$), the traces of Γ *vs.* t for the first five replications at both upwind stations with the corresponding traces for Ri = 0. In each replication at the lower upwind station for Ri = 10 the prominent first peak is caused by the arrival of the front of the heavily stratified cloud. This explains why the values of Γ at this peak are of order 5 times greater than in the other three cases shown in fig. 10 where, moreover, there is much

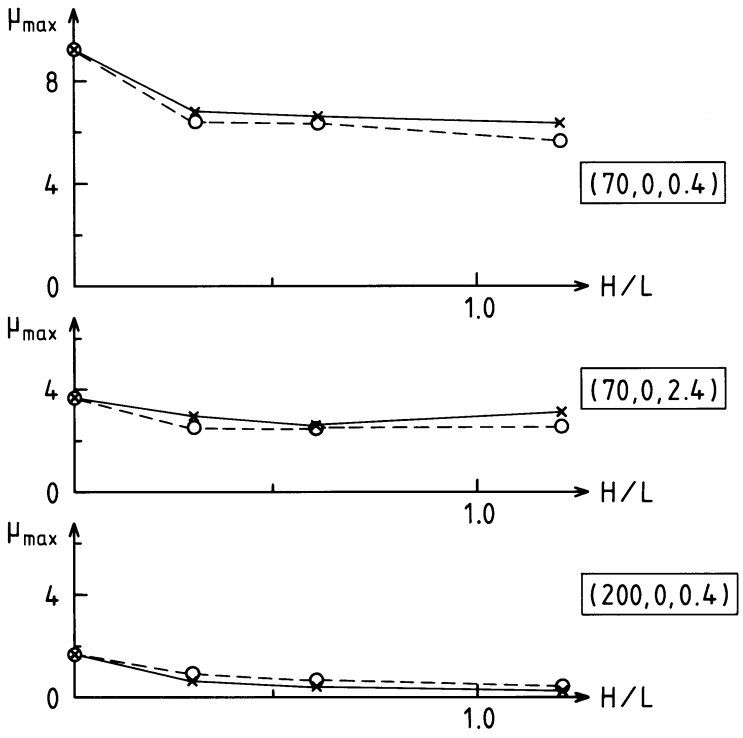

Fig. 9. – As for fig. 6, except that Ri = 2.

more irregularity. When Ri = 10, blocking upwind of the fence (for both solid and crenellated fences—see fig. 4) causes Γ to decay with t more slowly than when Ri = 0; Hall *et al.* [5] note that solid fences increase residence times. Figure 11 compares the graphs of μ *vs.* t at the two upwind stations for Ri = 10 and the highest fence with the corresponding graphs with no fence. The effects of stratification and blocking on the behaviour of μ are noticeable. Additionally, as noted above, the pronounced second maximum at the higher upwind station when the fence is present arises because the heavy cloud has to be lifted over the fence, and this effect is present to some extent for all fences as the second plot in fig. 12 shows. By contrast, the first plot in fig. 12 shows little effect on $\mu_{\max}$ of fences at the lower upwind sensor. At both downwind stations, the graph of μ against t is again always unimodal. Perhaps the most interesting feature of these plots is the more substantial reduction that fences cause at the lower downwind station, due, presumably, to the phenomenon noted above for heavy clouds not to slump after having been lifted over a fence; what is somewhat surprising, however, is that there is relatively little difference between solid and crenellated fences in this regard.

In summary and with some over-simplification, the main effect of fences of all sizes and types on the mean concentration μ is to reduce it because of increased mixing. This occurs for all Ri, and despite important differences in detail between solid and crenellated fences.

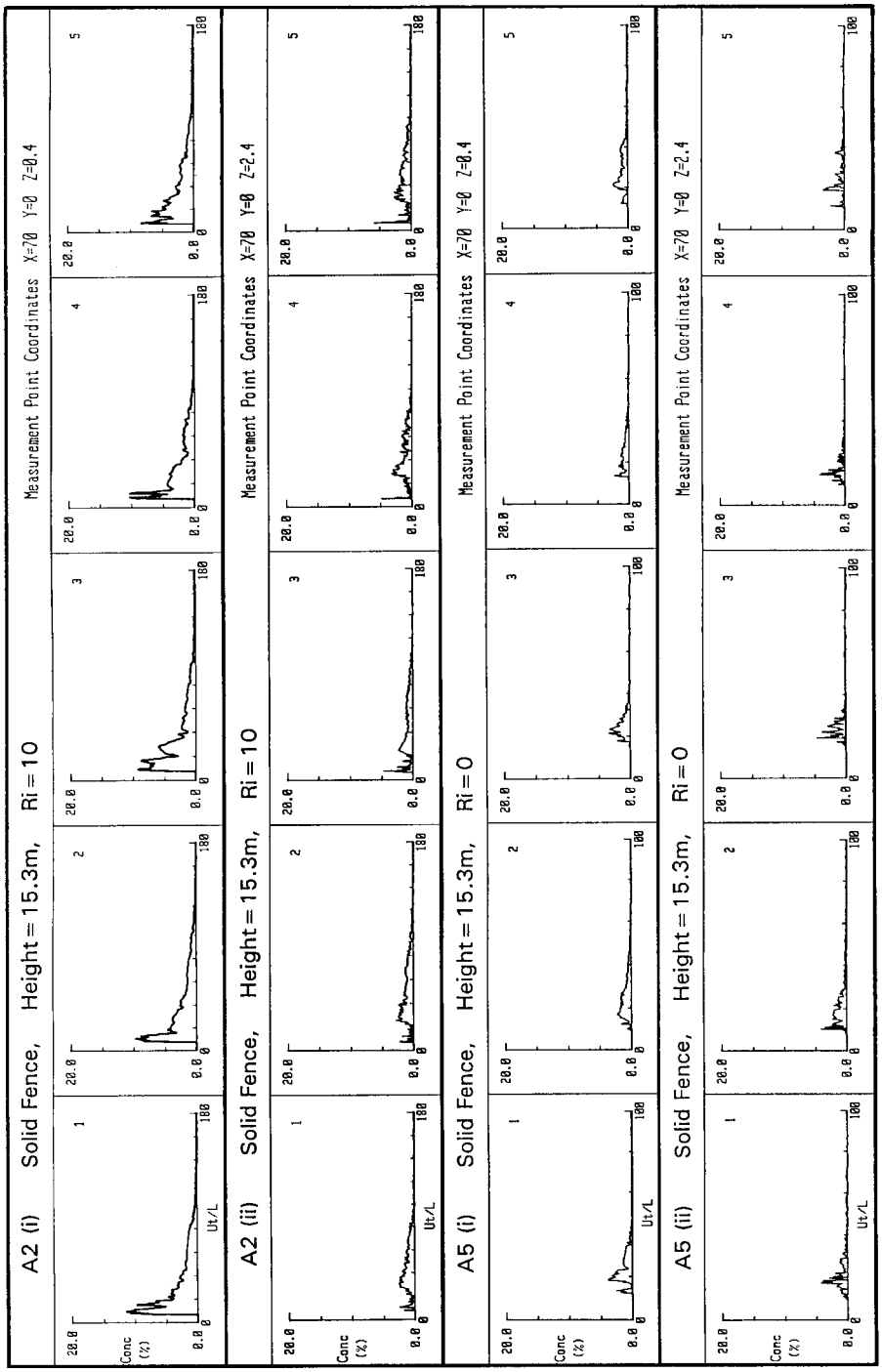

Fig. 10. – Comparisons of the time series for the first 5 replications when Ri = 10 with those for Ri = 0 at the two upwind stations in the presence of a solid fence with $H = 15.3$ cm. (a) Ri = 10, (70, 0, 0.4) cm. (b) Ri = 10, (70, 0, 2.4) cm. (c) Ri = 0, (70, 0, 0.4) cm. (d) Ri = 0, (70, 0, 2.4) cm.

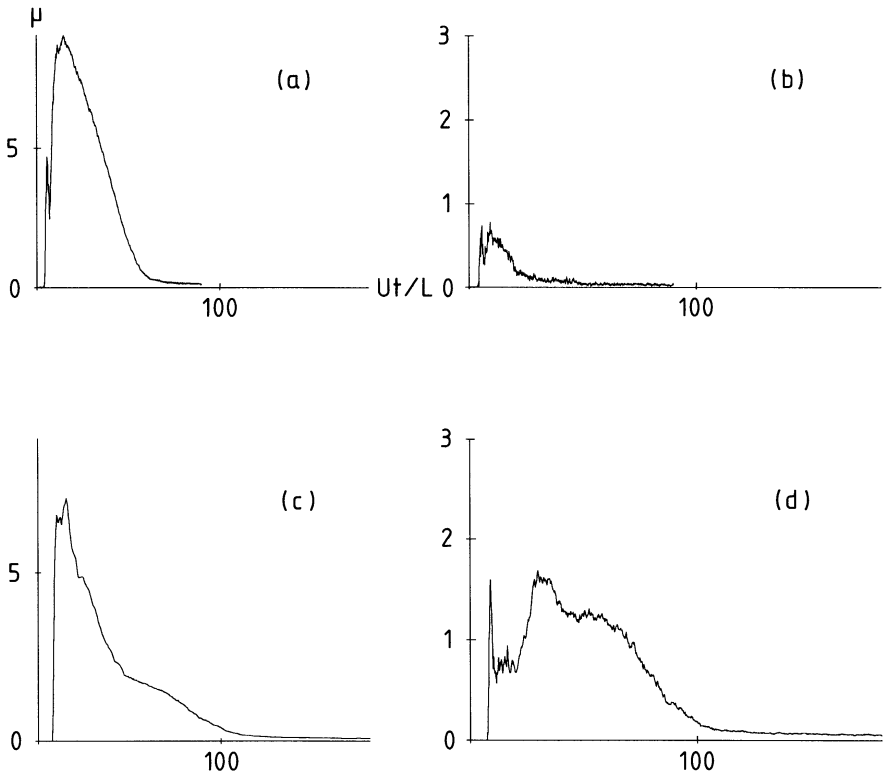

Fig. 11. – Ri = 10. Comparisons of μ (%) *vs.* Ut/L at both upwind stations for no fence with the highest solid fence. (a) No fence, (70, 0, 0.4) cm. (b) No fence, (70, 0, 2.4) cm. (c) Solid fence, $H = 15.3$ cm, (70, 0, 0.4) cm. (d) Solid fence, $H = 15.3$ cm, (70, 0, 2.4) cm.

4·3. *The standard deviation σ and its relationship to μ.* – At each sensor station (with position $\mathbf{x}$) the standard deviation $\sigma = \sigma(\mathbf{x}, t)$ depends on time t, and is the standard measure of the expected deviation of the values of the concentration $\Gamma(\mathbf{x}, t)$ from its mean value $\mu(\mathbf{x}, t)$. It has been noted above in discussing μ that the dominant effect of fences of all types is to tend to increase mixing, *i.e.* to tend to reduce the values of $\Gamma(\mathbf{x}, t)$ relative to their corresponding values when there are no fences. As fig. 6, 9 and 12 indicate, this normally reduces the mean, and would lead one to predict with some confidence that values of $\sigma(\mathbf{x}, t)$ would normally be reduced by the fences to about the same extent as the mean.

This belief is confirmed by almost all the graphs of σ *vs.* t obtained in the present analysis [8]; only some illustrative plots are included here. Figure 13 shows plots of σ *vs.* t for the three cases illustrated for the mean in fig. 5. Although these plots are for Ri = 0, they illustrate one predominant feature present at all Ri, for all fences and at all four stations, namely that the maximum value $\sigma_{\max}$ of σ occurs at about the same time as the maximum in the mean occurs (or the first maximum when there are two). This illustrates the strong effect on μ and σ of the randomness of the cloud position, including arrival time [3]. (Note that this effect would cause non-zero values of σ even if the cloud were "perfectly" mixed which, of course, it is not.) Figure 14 shows the plots

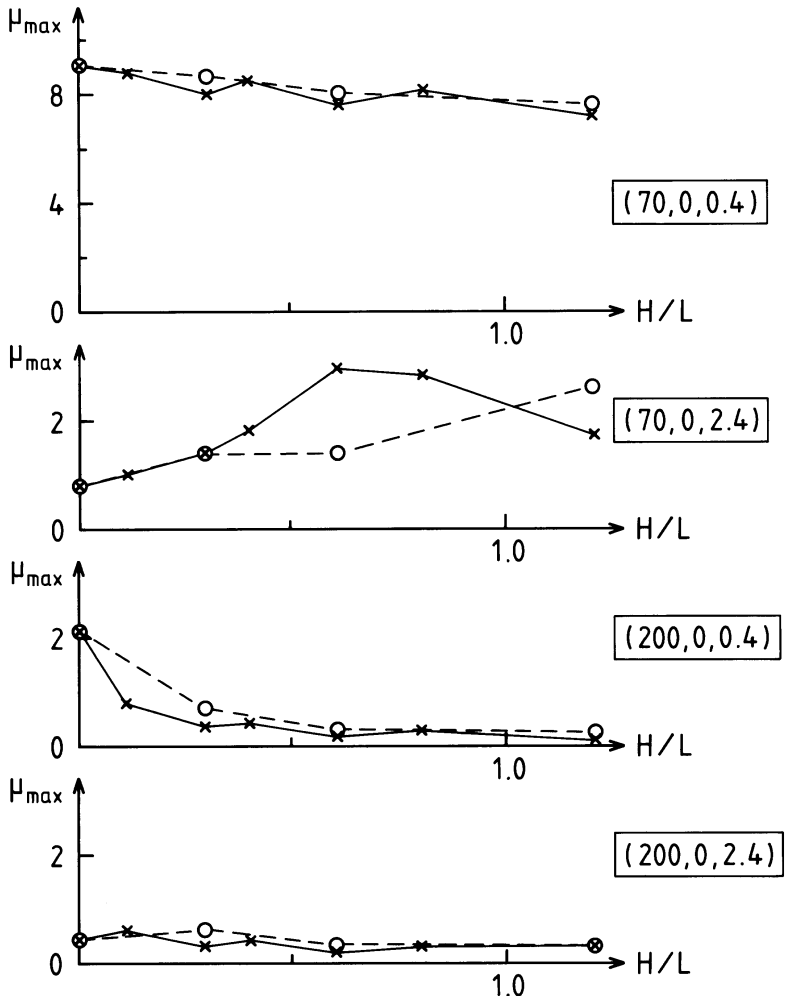

Fig. 12. – As for figs. 6 and 9, except that Ri = 10 and the behaviour at all 4 stations is shown.

of σ *vs.* t for the eight cases illustrated in fig. 8, all for Ri = 2 and all for upwind stations. They confirm the feature noted above, and also illustrate another prevalent property for heavy gas clouds when the plot of μ is bimodal. Compared with the plots of μ, the second maximum in the plots of σ is much reduced in size and the σ plot is also more spread about this peak. Both of these features seem very likely to be a result of the stronger effect on σ than on μ of the randomness of the cloud position. Finally, fig. 15 compares the μ and σ plots at downwind stations in three cases; these plots are typical.

The variations of $\sigma_{\max}$ with *H/L* are not shown here since, consistent with the predominant effect of mixing, they are very similar to those of $\mu_{\max}$ *vs. H/L*—see figs. 6, 9 and 12.

Chatwin and Sullivan [9] proposed a simple quadratic relationship between σ^2 and

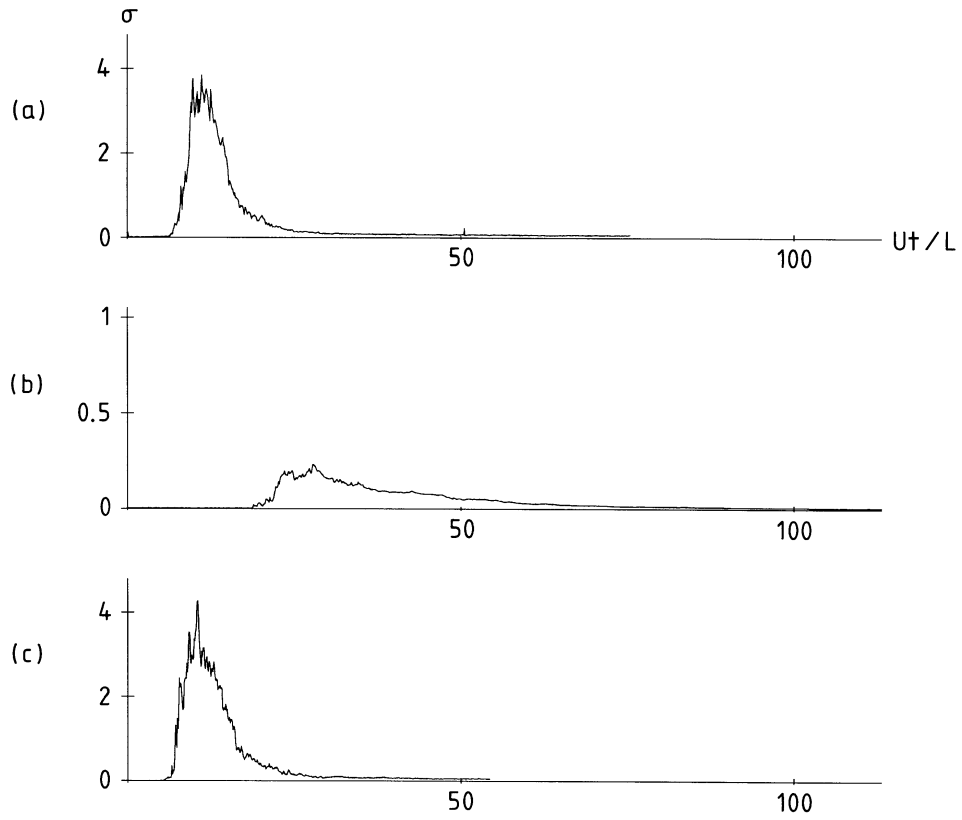

Fig. 13. – Plots of σ(%) *vs.* Ut/L for neutrally buoyant (Ri = 0) clouds for the three cases illustrated (for μ) in fig. 5.

μ, namely

$$\sigma^2 = \beta^2 \mu(\alpha\mu_0 - \mu), \tag{8}$$

where α and β are scalar non-dimensional parameters and μ_0 is a scale for μ (*e.g.* its maximum). They showed that eq. (8) fitted available data well, but the datasets were all taken for release from steady continuous sources in steady laboratory flows in conditions such that the statistical properties of the concentration field were self-similar and stationary. In these conditions both α and β must be constants, and the observed values satisfied $1 < \alpha < 3$ and $0 < \beta < 1$. It has since been shown that eq. (8) can be applied to model other datasets involving non-self-similar concentration fields [10] and non-uniform sources [11], but the concentration field was still statistically stationary; in these cases α and β were found, as expected, to be functions of downwind distance x, but slowly varying functions. These successes, and the generality of the underlying physical arguments on which eq. (8) was based, make it natural to try to apply it to other situations with time-varying sources. In these circumstances α, β (and μ_0) must be functions of **x** and t.

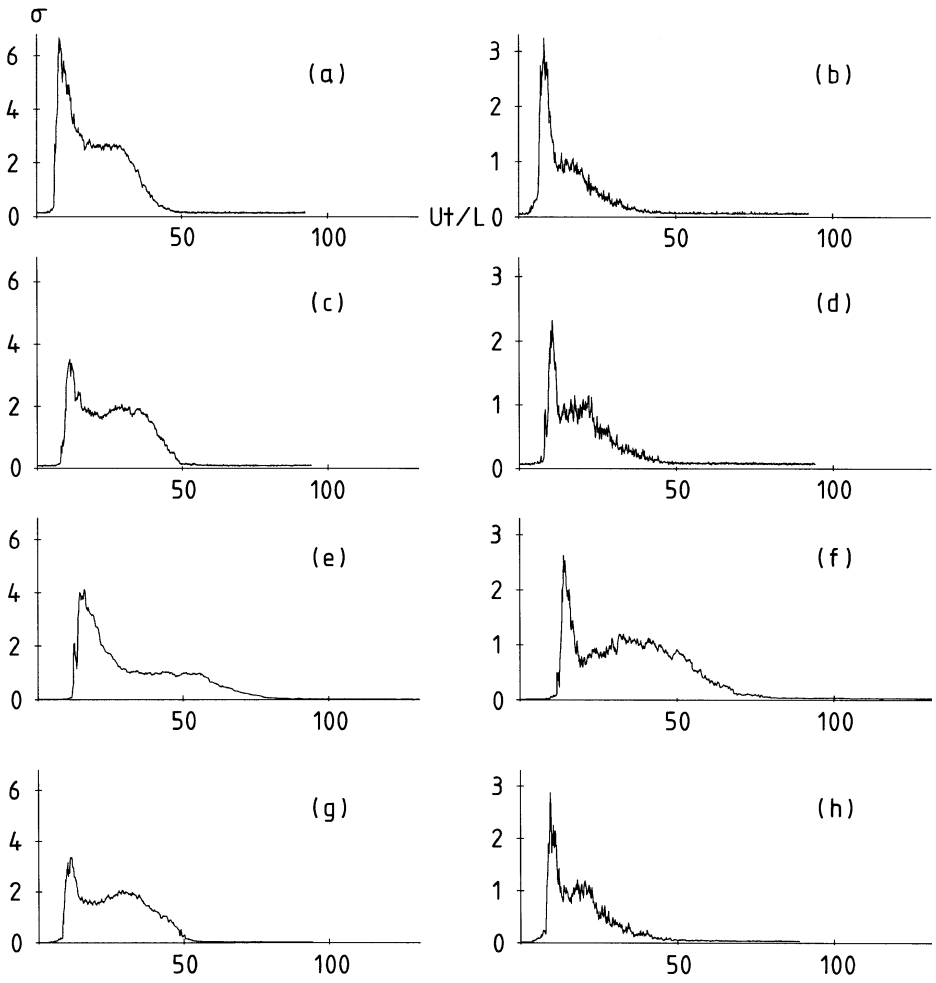

Fig. 14. – Ri = 2. Plots of σ (%) *vs.* Ut/L for the eight cases considered (for μ) in fig. 8.

Zimmerman and Chatwin [3] showed plots of σ^2 *vs.* μ for the no fence data of Hall *et al.* [1]—their figs. 5 and 6. As noted above, the plots of σ^2 *vs.* μ for all four stations and for all 33 cases shown in table I are given in [8]. Some typical plots are shown in fig. 16. Subject to the inevitable statistical noise, the plots are all closed loops, with the "sparser" upper loop corresponding to early times. This is consistent with the observations for no fence data made by Zimmerman and Chatwin [3]. Some trends were tentatively observed. As Ri increases, the bottom part of the loop tends to become more horizontal and there is a tendency for the loop to collapse, especially at the two higher stations. The latter tendency is also more prominent as fence height increases (although this is not shown in fig. 16). The data therefore appear to be consistent with some relationship between σ and μ, but it cannot be asserted at all that it is of the form in eq. (8), given that α, β and μ_0 must depend on each of $\mathbf{x}$, t, Ri and fence height and type. It is of interest to note, however, that eq. (8) predicts that, for fixed α and β, the

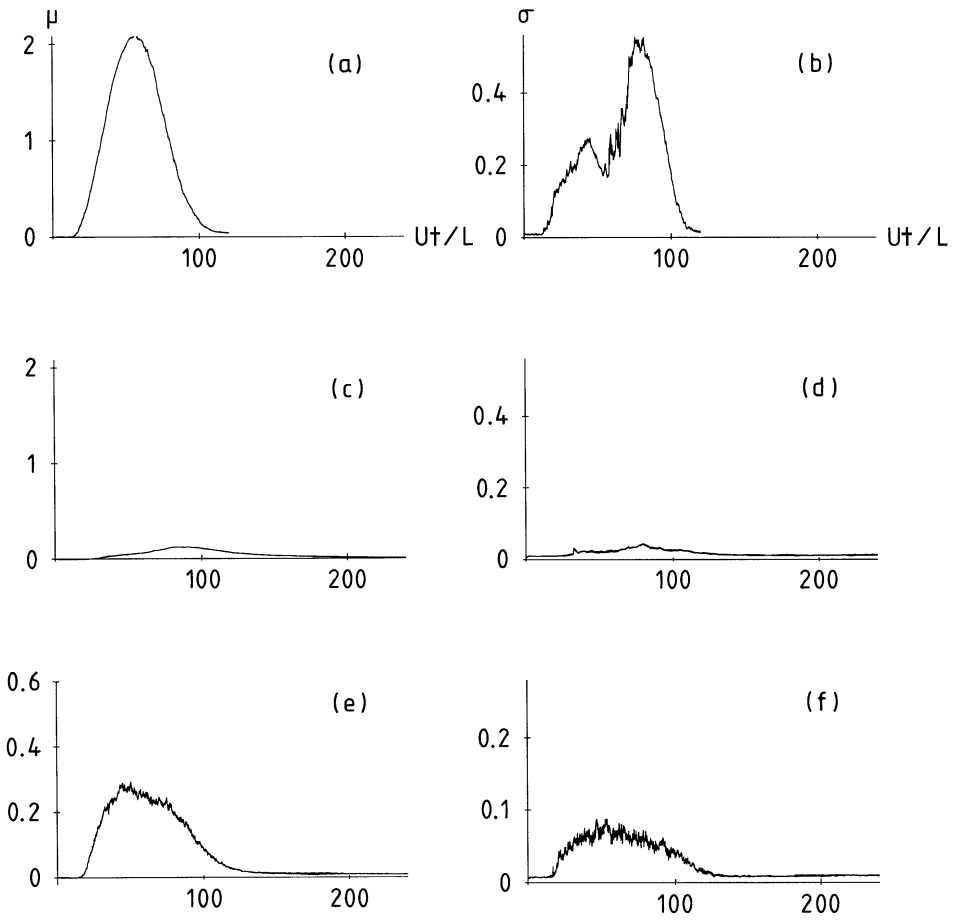

Fig. 15. – Ri = 10. Some typical plots of μ ((a), (c), (e)) and σ ((b), (d), (f)) *vs.* Ut/L at the downwind stations. (The units for μ and σ are %.) (a) and (b) no fence, (200, 0, 0.4) cm. (c) and (d) solid fence, H = 15.3 cm, (200, 0, 0.4) cm. (e) and (f) crenellated fence, H = 7.6 cm, (200, 0, 2.4) cm.

maximum value of σ/μ_0 is $(1/2)\alpha\beta$ (for $\alpha < 2$). For the data considered in [9], this gives values of σ/μ_0 from 0.22 to 0.46. The values of σ/μ for the present data are all of order unity or somewhat less so it can at least be said that there is no obvious contradiction with eq. (8)! Mole [12] intends to develop mathematical models of α and β, using the approach introduced by Moseley [13] and taken further in Mole [14]. See also Clarke and Mole [15].

4·4. *The skewness and kurtosis, and the* (K, S) *plots.* – After μ and σ, the next two parameters in the hierarchy of central moments $\{\mu_n\}$—see eq. (6)—are μ_3 and μ_4, instead of which it is more common to use the non-dimensional measures skewness S and kurtosis K, defined in eq. (7). With the limited number of replications available, the statistical noise present in their estimates is quite large and noticeably greater than in those of μ and σ. This is illustrated by the two typical plots in fig. 17, which show three features present in (nearly) all plots. These are:

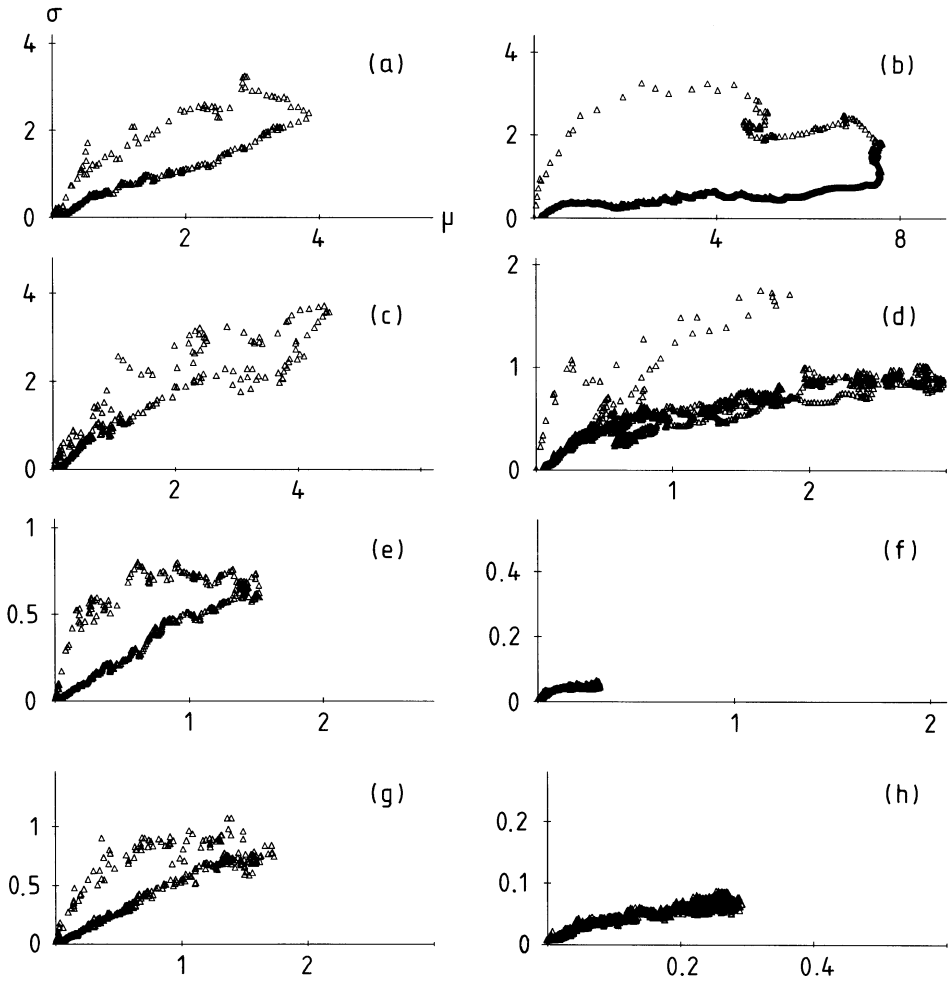

Fig. 16. – Some typical (σ, μ) plots. (In all cases the ordinate and abscissa are σ and μ, respectively.) Solid fence, $H = 7.6$ cm, (70, 0, 0.4) cm. (a) Ri = 0, (b) Ri = 10. Solid fence, $H =$ 7.6 cm, (70, 0, 2.4) cm. (c) Ri = 0, (d) Ri = 10. Crenellated fence, $H = 7.6$ cm, (200, 0, 0.4) cm. (e) Ri = 0, (f) Ri = 10. Crenellated fence, $H = 7.6$ cm, (200, 0, 2.4) cm. (g) Ri = 0, (h) Ri = 10.

i) An irregular period at the beginning of the record. This is due to noise and contributes most, but not all, of the negative values of S; recall that $S = 0$ for PDFs that are symmetric about their means such as the Normal distribution. There is also an irregular period at the end of the record with somewhat different properties; for example, the values of S are mainly positive. This corresponds to slowly moving residual gas which Sweatman and Chatwin [4] showed to be present for the no fence data, and to have significant effects on the dosages; see the comment on positive values of S in ii) immediately below.

ii) The largest positive maximum in the estimates of S occurs substantially before the first maximum in μ. Since large positive values of S arise from PDFs dominated by

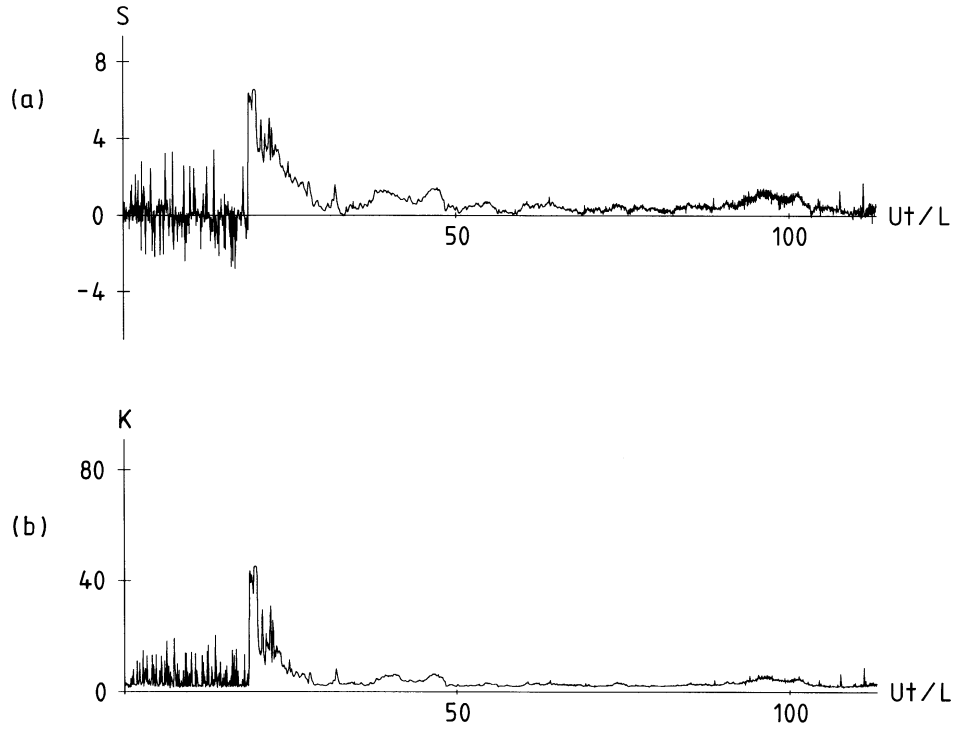

Fig. 17. – Typical plots of estimates of (a) skewness S, and (b) kurtosis K, against Ut/L. The plots are for Ri = 0, solid fence with $H = 15.3$ cm at (200, 0, 0.4) cm.

high probabilities of low concentrations but with long tails representing low probabilities of much higher concentrations, this observation is consistent with the bulk of the cloud not having reached the sensor in most replications, but that there are a few replications in which it has arrived. In other words, this maximum in S is associated with the randomness in cloud arrival times already noted above as a principal contribution [3].

iii) The plots of K tend to track rather closely the corresponding plots of S although, of course, K is always positive.

The last feature is common to many other datasets ([3, 16, 17]). For all of these, analyses in the quoted papers have shown that, with due account taken of statistical noise and experimental error, the plot of K against S collapsed onto a single quadratic curve of the form

$$K = aS^2 + b\,, \tag{9}$$

where theory well-known to statisticians, and discussed in the present context by Mole and Clarke [16] shows that the constants a and b are such that $K > S^2 + 1$ and, moreover, that all the individual points must also satisfy this inequality.

This remarkable collapse onto a parabola has been confirmed for *all* the datasets considered in the present paper. (Zimmerman and Chatwin [3] had already examined

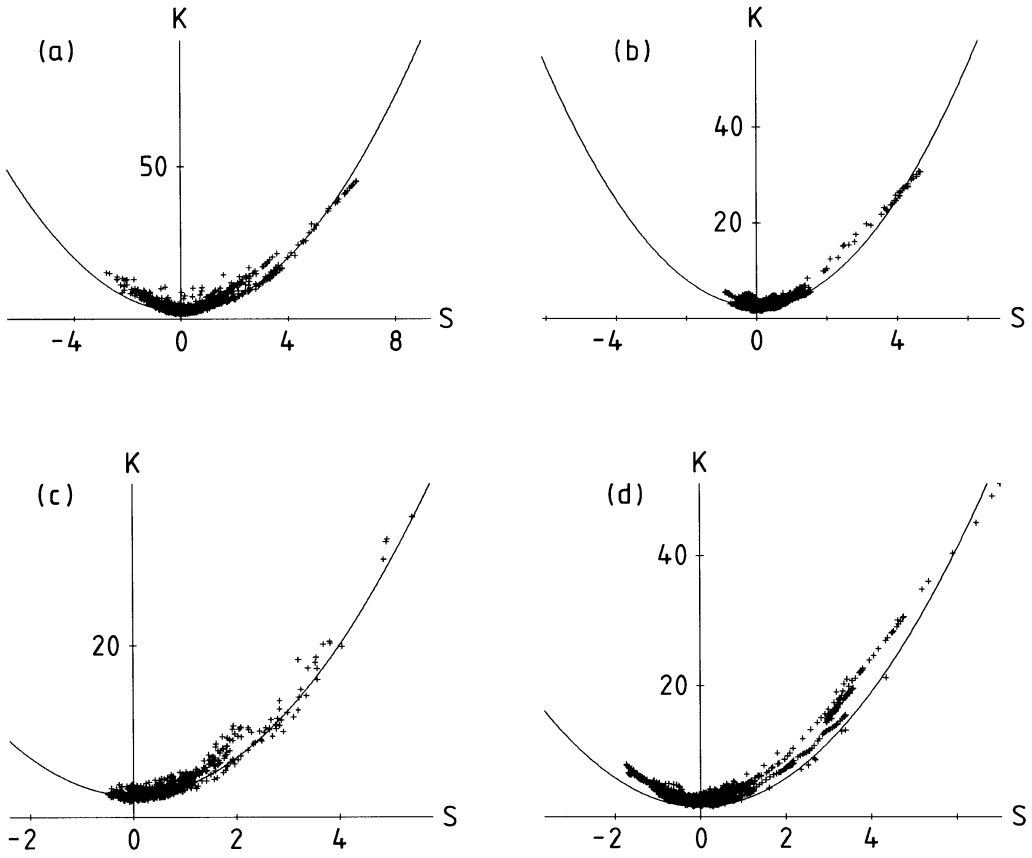

Fig. 18. – Four typical (K, S) plots, with the solid curve being the fitted quadratic $K = aS^2 + b$—see table II for values of (a, b). (In all cases the ordinate and abscissa are K and S, respectively.) (a) Ri = 0, solid fence, H = 15.3 cm, (200, 0, 0.4) cm. (b) As in (a) except that Ri = 10. (c) Ri = 0, crenellated fence, H = 7.6 cm, (70, 0, 0.4) cm. (d) As in (c) except that Ri = 10.

the no fence data.) All plots are given in [8], and four typical ones are shown here in fig. 18 together with, in each case, a fitted quadratic of the form in eq. (9). All the points lie above $K = S^2 + 1$. In general, the collapse is best for low Ri. For large Ri, the collapse is good for the two upwind sensors regardless of the presence, height or type of fence; downwind there is a tendency which increases as fence height increases for the points to clump together at the bottom of the curve. Table II lists all the (a,b) values for the fitted quadratics (including the no fence data). Although Robinson [8] identifies some trends in the variation of these values with Ri, and fence height and type, the overwhelming impression is that they are remarkably unvarying.

As has been explained in detail elsewhere by Mole and Clarke [16] and Mole [14], the physical arguments that predict the collapse of the (K, S) plot onto a parabola can be developed in an obvious way. As noted also in these papers, an important implication is that, for practical purposes at least, $p(\theta; \mathbf{x}, t)$ is determined by three quantities only, *e.g.*, $\mu(\mathbf{x}, t)$, $\sigma(\mathbf{x}, t)$ and $S(\mathbf{x}, t)$.

TABLE II. – *Values of* (a, b) *in eq.* (9). *The notation* (A), (B), (C), (D) *denotes the stations at* (70, 0, 0.4) cm, (70, 0, 2.4) cm, (200, 0, 0.4) cm, (200, 0, 2.4) cm, *respectively*.

		Ri	0	1	2	5	10
	no fence		(1.2, 2.5)	(1.25, 2.0)	(1.2, 2.5)	(1.1, 2.1)	(1.0, 2.0)
	(S)	1.6	—	—	—	—	(1.1, 2.0)
	solid fence	3.8	—	(1.2, 2.4)	(1.2, 2.5)	(1.1, 2.1)	(1.1, 2.0)
	(height/cm)	5.1	(1.1, 2.5)	—	—	—	(1.1, 2.0)
		7.6	(1.1, 2.5)	(1.2, 2.4)	(1.2, 2.5)	(1.1, 2.1)	(1.1, 1.5)
(A)		10.2	(1.1, 2.5)	—	—	—	(1.1, 1.5)
		15.3	(1.1, 2.5)	(1.25, 2.0)	(1.2, 2.5)	(1.1, 2.1)	(1.1, 1.5)
	(C)	3.8	(1.1, 2.5)	—	(1.2, 2.5)	—	(1.1, 1.5)
	crenellated fence	7.6	(1.1, 2.5)	—	(1.2, 2.5)	—	(1.1, 1.5)
	(height/cm)	15.3	(1.1, 2.5)	—	(1.2, 2.5)	—	(1.1, 1.5)
	no fence		(1.2, 2.5)	(1.5, 2.5)	(1.2, 3.0)	(1.1, 2.0)	(1.1, 2.5)
	(S)	1.6	—	—	—	—	(1.1, 2.5)
	solid fence	3.8	—	(1.2, 2.1)	(1.2, 2.5)	(1.1, 2.0)	(1.1, 2.5)
	(height/cm)	5.1	(1.1, 2.5)	—	—	—	(1.1, 2.5)
		7.6	(1.1, 2.5)	(1.2, 2.1)	(1.2, 2.5)	(1.1, 2.0)	(1.1, 2.5)
(B)		10.2	(1.1, 2.5)	—	—	—	(1.1, 2.5)
		15.3	(1.1, 2.5)	(1.5, 2.5)	(1.1, 2.5)	(1.1, 2.0)	(1.1, 2.5)
	(C)	3.8	(1.1, 2.5)	—	(1.2, 2.5)	—	(1.2, 2.5)
	crenellated fence	7.6	(1.1, 2.5)	—	(1.2, 2.5)	—	(1.2, 2.5)
	(height/cm)	15.3	(1.1, 2.5)	—	(1.2, 2.5)	—	(1.1, 2.5)
	no fence		(1.1, 2.5)	(1.25, 2.5)	(1.2, 2.5)	(1.1, 2.5)	(1.3, 2.5)
	(S)	1.6	—	—	—	—	(1.1, 2.5)
	solid fence	3.8	—	(1.25, 2.5)	(1.2, 2.5)	(1.1, 2.5)	(1.3, 2.5)
	(height/cm)	5.1	(1.1, 2.5)	—	—	—	(1.3, 2.5)
		7.6	(1.1, 2.5)	(1.25, 2.5)	(1.2, 2.5)	(1.2, 2.5)	(1.4, 2.5)
(C)		10.2	(1.1, 2.5)	—	—	—	(1.4, 2.5)
		15.3	(1.1, 2.5)	(1.25, 2.5)	(1.2, 2.5)	(1.3, 2.5)	(1.4, 2.5)
	(C)	3.8	(1.1, 2.5)	—	(1.3, 2.5)	—	(1.3, 2.5)
	crenellated fence	7.6	(1.1, 2.5)	—	(1.1, 2.5)	—	(1.4, 2.5)
	(height/cm)	15.3	(1.1, 2.5)	—	(1.1, 2.5)	—	(1.4, 2.5)
	no fence		(1.2, 2.5)	(1.25, 2.5)	(1.4, 2.5)	(1.2, 2.0)	(1.3, 2.5)
	(S)	1.6	—	—	—	—	(1.25, 2.5)
	solid fence	3.8	—	(1.25, 2.5)	(1.1, 2.5)	(1.1, 2.0)	(1.5, 2.5)
	(height/cm)	5.1	(1.1, 2.5)	—	—	—	(1.5, 2.5)
		7.6	(1.1, 2.5)	(1.25, 2.5)	(1.1, 2.5)	(1.2, 2.0)	(1.5, 2.5)
(D)		10.2	(1.1, 2.5)	—	—	—	(1.5, 2.5)
		15.3	(1.0, 2.5)	(1.25, 2.5)	(1.4, 2.5)	(1.2, 2.0)	(1.5, 2.5)
	(C)	3.8	(1.1, 2.5)	—	(1.1, 2.5)	—	(1.25, 2.5)
	crenellated fence	7.6	(1.1, 2.5)	—	(1.1, 2.5)	—	(1.25, 2.5)
	(height/cm)	15.3	(1.1, 2.5)	—	(1.1, 2.5)	—	(1.25, 2.5)

5. – Conclusions

Although some important variations of the statistical properties with fence type and height have been identified, the main conclusion is perhaps that such variations are, in practice, less important than those caused by the presence of a fence of any type or height. There are good prospects for modelling the PDF, but any mathematical model must be tested against reliable experimental estimates and these require many replications of a single configuration, rather than relatively few replications of numerous configurations as for the data considered here.

* * *

It is a pleasure to thank DAVID HALL for his great help. This work was supported by the European Union.

REFERENCES

[1] HALL D. J., WATERS R. A., MARSLAND G. W., UPTON S. L. and EMMOTT M. A., Report No. LR 804 (PA), Warren Spring Laboratory (1991).
[2] DAVIES J. K. W., *J. Haz. Mat.,* **31** (1992) 177.
[3] ZIMMERMAN W. B. and CHATWIN P. C., *Boundary-Layer Meteorol.,* **75** (1995) 321.
[4] SWEATMAN W. L. and CHATWIN P. C., *Boundary-Layer Meteorol.,* **77** (1996) 211.
[5] HALL D. J., KUKADIA V., UPTON S. L., MARSLAND G. A. and EMMOTT M. A., Report No. LR 805 (PA), Warren Spring Laboratory (1991).
[6] MCQUAID J. (Editor), *J. Haz. Mat.,* **11** (1985) Special Issue.
[7] DERKSEN R. W. and SULLIVAN P. J., *Comb. & Flame,* **81** (1990) 378.
[8] ROBINSON C., Report No. TR/01/96, School of Mathematics and Statistics, University of Sheffield (1995) (with 5 Appendices).
[9] CHATWIN P. C. and SULLIVAN P. J., *J. Fluid Mech.,* **212** (1990) 533.
[10] CHATWIN P. C., SULLIVAN P. J. and YIP H., in *Proceedings of the International Conference on Physical Modelling of Transport and Dispersion*, edited by E. E. ADAMS and G. E. HECKER (M.I.T.) 1990, pp. 6B3-6B8.
[11] SAWFORD B. L. and SULLIVAN P. J., *J. Fluid Mech.,* **289** (1995) 141.
[12] MOLE N., personal communication (1996).
[13] MOSELEY D. J., M. Sc. Dissertation, University of Western Ontario (1991).
[14] MOLE N., *Environmetrics,* **6** (1995) 559.
[15] CLARKE E. D. and MOLE N., *Environmetrics,* **6** (1995) 607.
[16] MOLE N. and CLARKE E. D., *Boundary-Layer Meteorol.,* **73** (1995) 35.
[17] LEWIS D. M. and CHATWIN P. C., *Environmetrics,* **6** (1995) 583.